Synthesis and target annotation of GB18

Stone Woo[1,2] and Ryan A. Shenvi[1]*

[1]Department of Chemistry, Scripps Research, 10550 North Torrey Pines Road, La Jolla, California 92037, United States.
[2]Skaggs Graduate School of Chemical and Biological Sciences

Ingestion of alkaloid metabolites from the bark of *Galbulimima* (GB) *sp*. leads to psychotropic and excitatory effects in humans. Only a single target, the muscarinic acetylcholine receptor, has been assigned. Limited, variable supply of GB alkaloids has impeded their biological exploration and clinical development. Here we report a solution to the supply of GB18, a structural outlier and putative psychotropic principle of *Galbulimima* bark. Efficient access to the challenging tetrahedral attached-ring motif required the development of a ligand-controlled *endo*-selective cross-electrophile coupling and a diastereoselective hydrogenation of a rotationally-dynamic pyridine. Reliable, gram-scale access to GB18 allowed its assignment as a potent antagonist of *kappa*- and *mu*- opioid receptors and lay the foundation to navigate and understand the biological activity of *Galbulimima* metabolites.

The GB alkaloids[1] derive from the bark of *Galbulimima sp*., which features in the traditional medicine and ritual of Papua New Guinea as an analgesic, antipyretic and hallucinogen.[2-5] Forty alkaloids unique to *Galbulimima* comprise four structural classes differentiated by connectivity between conserved piperidine and decalin motifs (Classes I-IV, see Figure 1). Of twelve alkaloids subjected to in vivo assays, ten elicited diverse physiological or behavior changes in mammals at or below 10 mg/kg.[6] Most affected heart rate, blood pressure or muscle spasm. The most potent antispasmotic, himbacine (Class I) garnered the most interest as a candidate for treatment of bradycardia (abnormally slow heart beat),[7] Alzheimer's disease[8–10] and intraocular pressure[11] due to its potent antagonism of muscarinic acetylcholine receptor (mAChR) M_2 (K_d = 4 nM).[7] Only a single alkaloid displayed activity consistent with effects on behavior. GB18 inhibited mouse preening at 5 mg/kg, with no effect on pain threshold, which was interpreted as an effect on cognition instead of sensation.[6] A high potency target was not identified. GB18 is not widely available and its abundance in *Galbulimima* bark is not reported. However, the extreme variability of overall alkaloid content and ratio, unrelated to location and season (0.5% to trace total alkaloid content, *avg*. content 57 ppm, excluding the abundant alkaloid, himbacine)[12,13] frustrated re-isolation attempts, leading to ad hoc procedures for extraction and purification.[12] GB18 and himbacine both correspond to Class I alkaloids (subclassified here as Ia and Ib). Synthesis of GB18 would allow comparison to himbacine and correlation of changes in structure (see Figure 1) and function (tachycardia vs. preening inhibition) with changes to receptor affinity and selectivity. This change in structure corresponds to alteration of the pendant piperidine ring of himbacine to the tetrahedral attached-ring of GB18 and alters the problem of synthesis significantly.

Access to GB18 via chemical synthesis is challenged by the strained ether in its core and vicinal, stereogenic attached-ring bridgeheads that position the piperidine into the concave face of the oxa-tetracycle. Retrosynthetic cleavage of the attached-ring bridge to a β-haloether reduces Böttcher complexity by 28% (448 to 325 mcbits)[14] but control of bridgehead stereochemistry does not benefit from analogy in the literature. The attached-pyridine (**2**) can undergo facile bond rotation (see SI) to expose either face for hydrogenation, in contrast to

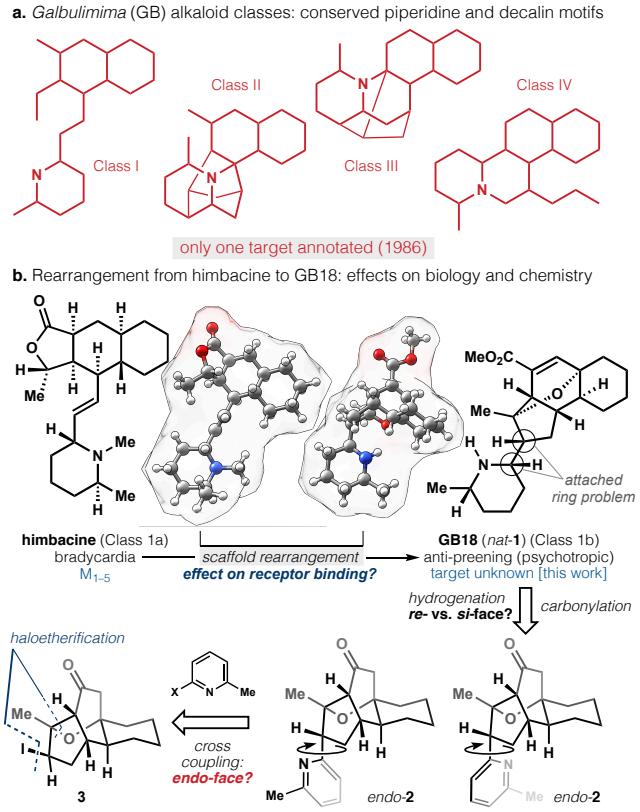

Figure 1. Analysis of structure and synthesis. **a.** GB alkaloids are classified by piperidine/decalin topology (in red) but a target has only been assigned to the most abundant alkaloid, himbacine. **b**. The pendant piperidine of himbacine is rearranged to an attached-ring system, which challenges stereocontrol.

the rigid GB scaffolds explored previously.[15,16] Stereoselective appendage of the pyridine onto the carbocyclic core must overcome the steric repulsion of the *endo*-face (*endo*-**2** is destabilized 0.5 kcal/mol vs. its *exo*-isomer, MM2) and the tendency of the bridging ether to fragment at either carbon (*vide infra*). The simplicity offered by this approach, however, mitigated its inherent risk. Cross-coupling substrate **3** might be accessed by haloetherification, which keyed the use of a Danheiser annulation transform to the unencumbered convex face of enone **4** (see Figure 2) and simplified the entry. Execution on multigram scale validated this design (2.5 g of *rac*-GB18 was prepared). Access to *nat*-GB18 allowed its annotation as a potent antagonist for *kappa*- (9 nM IC_{50}) and *mu*-opioid (12 nM IC_{50}) receptors.

A robust entry was available via **5**, the Robinson annulation product of cyclohexanone and methyl vinyl ketone. Conjugate borylation using catalytic Cu(I)-CyJohnPhos accessed *cis*-decalone **6** stereoselectively in one step on small scale (see SI), but a two-step protocol of hydrogen peroxide-mediated epoxidation[17] and palladium-catalyzed hydrogenation[18] yielded 29.4 grams (175 mmol) of **6** in one pass. Identification of a solvent system (1:1 EtOAc:HFIP) that decreased hydrogenation catalyst loading (1% Pd/C vs. 10% in EtOAc alone), minimized overreduction and ensured reproducible yields on scale-up. High-yielding desaturation (91% yield, 2 steps) was achieved by regioselective (98:2 $\Delta^{2,3}$: $\Delta^{1,2}$) double silylation (**7**), followed by Saegusa oxidation (10% $Pd(OAc)_2$) under modified Larock conditions to provide a 71 wt% (^{1}H NMR) solution in PhMe of the volatile enone **4**. Danheiser annulation[19] proceeded with excellent stereoselectivity (concave-face diastereomer not detected) in the presence of 1.4 equiv. $TiCl_4$ to provide, initially, an alkenylsilane with *tert*-alkyl silyl ether intact. *In situ* addition of HFIP at -40 °C effected double desilylation to provide a 64% yield (^{1}H NMR) of **8**. A two-step annulation/ protodesilylation was ineffective using fluoride (e.g. TBAF, BF_3•Et_2O) or alkoxide-based (K_2CO_3/MeOH) protocols due to the tendency of **8** to isomerize and/or eliminate water, necessitating the *in situ* alkenylsilane protodesilylation protocol, which may rely on a transient $Ti(HFIP)_nCl_m$-substrate complex (see SI). Scale-up of this sequence from cyclohexanone was aided by identification of crystalline intermediates (SI-**2**, **6** and **8**), which allowed single-pass isolation of 13.4 g of **8** (98% purity, ^{1}H NMR) with only one filtration through silica (the reaction mixture containing **4**, 2 M in DMSO, was eluted from SiO_2 1:13 (w:w) without prior workup). Sensitivity of **8** to acid and base also frustrated haloetherification with a range of halonium sources (e.g. NCS, Palau'chlor, NBS, DBDMH, TBCHD, see SI). In contrast, iodoetherification using NIS in HFIP delivered bridging ether **3** (confirmed by X-ray) on multigram scale (5.6 g, 82%), which possessed the tetracyclic core of **1**. Establishment of the *endo*-attached-ring motif with a large heterocyclic partner promised to be challenging, however. The primary strategy of C–I bond homolysis was probed by Giese addition of the C-radical (see Figure 2) to methyl propiolate or phenyl vinyl sulfone but was unsuccessful. Only solvent quantities of the small radicalophile, TMS-acetylene, proved competent to trap the radical derived from **3** and produced a near equimolar ratio of diastereomers favoring *exo*-**9**. Comparable reactivity with heterocycles proved elusive.

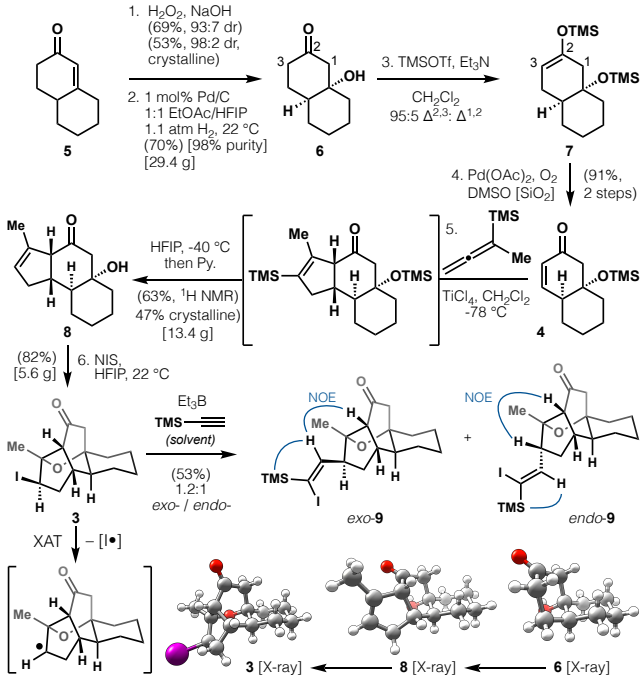

Figure 2. Entry into the GB18 core identifies low selectivity associated with radical addition reactions.

Minisci-type addition to 2-picoline, 2-picoline N-oxide or N-methoxy-2-picolinium acceptors[20] yielded no attached-rings and transition metal-mediated cross-coupling (Pd, Ni, Fe)[21] between **3** and metastable C2-metalated-pyridines (Mg, Zn)[22] produced complex mixtures with no detectable product. Sensitivity of the strained β-iodo ether of **3** prompted a search for more chemoselective conditions. Cross-electrophile coupling has emerged as a widely adopted tool[23] since seminal contributions over the last decade by Weix, Reisman, and others,[24,25] but has not seen use for stereoselective attached-ring coupling. Attempts to leverage photoredox catalysis[26] yielded only traces of desired product amidst complex mixtures, possibly due to the photosensitivity of **3**, which darkened over several hours under ambient laboratory light. Modified Weix conditions for Ni-catalyzed heteroaryl reductive coupling[27] with 6-bromo-2-picoline also gave low levels of *endo*-**2**, but byproducts were few and identifiable, aiding optimization efforts. Off-pathways included homodimerization (to 6,6'-dimethyl-2,2'-bipyridine), E1cB ether fragmentation (**13**), deiodinative ether fragmentation (**14**) and protodehalogenation of **3**. Fragmentation byproduct **14** reflected the strain of the oxygen bridge, its instability and tendency to eliminate, and was favored with Zn^0, Mn^0 and TDAE[28-29] as reductants for Ni, restricting the options available for cross-electrophile coupling. We recently reported a suite of alkene hydrofunctionalizations that merged metal-hydride hydrogen atom transfer (MHAT) catalysis with nickel cross-coupling cycles,[30] where the MHAT catalyst itself appeared necessary for reduction of Ni^{2+} to Ni^{1+}.[31,32] Adaptation of this reducing system ($Mn(dpm)_3$/$PhSiH_3$) for production of **2** yielded the most promising results (Figure 3).[33] Exhaustive screening identified an optimal combination of pyridine electrophile (6-iodo-2-picoline), solvent (DMA), exogenous base (0.03 M Li_2CO_3), temperature (35 °C), salt (0.4 M NaI) and Ni source (0.06 M $NiBr_2$•diglyme). Weix-type amidine ligands[34] and previously unexplored amidines provided variable

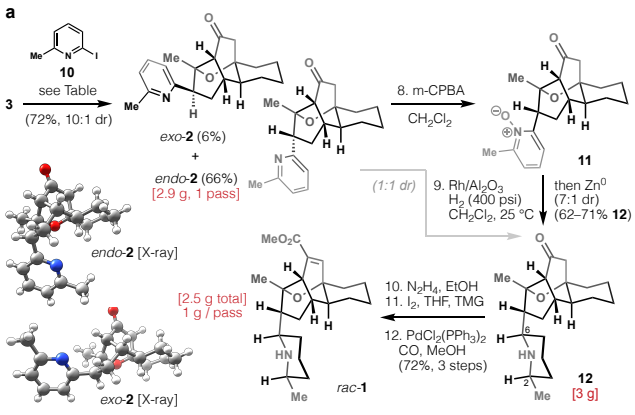

b

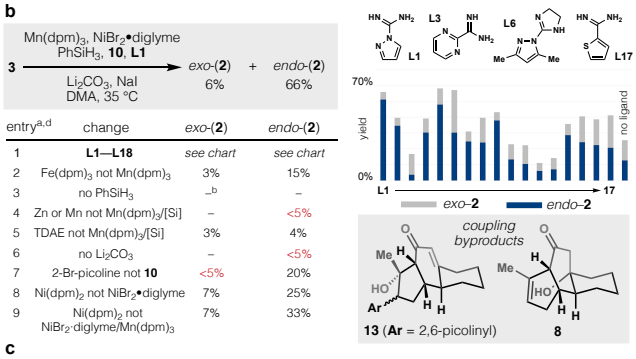

entry[a,d]	change	exo-(2)	endo-(2)
1	**L1—L18**	*see chart*	*see chart*
2	$Fe(dpm)_3$ not $Mn(dpm)_3$	3%	15%
3	no $PhSiH_3$	–[b]	–
4	Zn or Mn not $Mn(dpm)_3$/[Si]	–	<5%
5	TDAE not $Mn(dpm)_3$/[Si]	3%	4%
6	no Li_2CO_3	–	<5%
7	2-Br-picoline not **10**	<5%	20%
8	$Ni(dpm)_2$ not $NiBr_2$•diglyme	7%	25%
9	$Ni(dpm)_2$ not $NiBr_2$·diglyme/$Mn(dpm)_3$	7%	33%

c

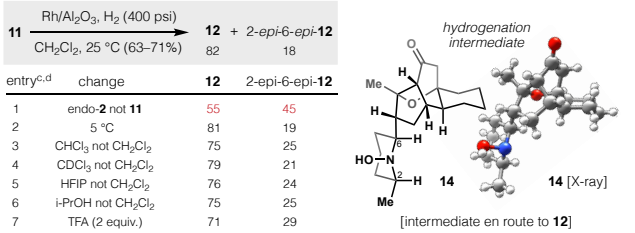

entry[c,d]	change	12	2-epi-6-epi-12
1	endo-**2** not **11**	55	45
2	5 °C	81	19
3	$CHCl_3$ not CH_2Cl_2	75	25
4	$CDCl_3$ not CH_2Cl_2	79	21
5	HFIP not CH_2Cl_2	76	24
6	i-PrOH not CH_2Cl_2	75	25
7	TFA (2 equiv.)	71	29

Figure 3. Completion of *rac*-**GB18** (*rac*-**1**) on gram scale. **a**. Control of attached-ring bridgeheads enables a short, stereocontrolled route. **b.** Optimization of *endo*-selective cross-electrophile coupling; [a] 0.02 mmol scale; [b] – denotes no detected product by TLC or LCMS; [c] 0.005 mmol scale; [d]yields increased on preparative scales (>1.0 mmol). **c.** Optimization of diastereoselective pyridine hydrogenation via freely rotating attached-rings.

diastereoselectivity ranging from no preference (no ligand, **L6**, **L17**) to strong preference for *exo*-**2** (**L3**) (see Figure 3; full list of ligands in SI). A novel ligand proved to be the most selective and highest yielding: **L1**, 1*H*-pyrazole-1-carboxamidine (Praxidine), an inexpensive, commercially available ($50/100g, Combiblocks) guanidinylating reagent and anti-inflammatory, favored *endo*-**2** by over 10:1 versus *exo*-**2**. The mechanistic complexity of possible reducing/coupling pathways has frustrated the development of conditions that are catalytic in either Ni^{2+} or Mn^{3+}, and remains the subject of ongoing investigation. Nevertheless, the efficiency of the reaction allowed batch scale-up to 2.9 grams of **2** in a single pass from **3** (72%, 10:1 dr). The high diastereomeric ratio reflects a 1.4 kcal/mol difference between organometallic intermediates or transition states, which may derive from a hydrogen bond network between the pyridine-nickel-ligand complex and the Lewis basic oxygen bridge of **3** (see SI). *Endo*-**2** is destabilized by 0.5 kcal/mol vs. *exo*-**2** (MM2), and epimerization was not observed by resubjection of products to coupling conditions. These results demonstrate a surprising and, to the best of our knowledge, unprecedented reversal of stereoselectivity based on ligand structure to access the more hindered isomer of cross-electrophile coupling.

Endo-selective cross-electrophile coupling established one bridgehead stereocenter, but the attached-piperidine bridgehead presented a different challenge. The pyridine ring of **3** appeared to equally rotate each prochiral face to incoming reagents (see SI), resulting in *ca*. 1:1 dr upon hydrogenation. Strategies to lock the conformation of the ring—pyridine protonation, hydrogen bond donors, chelating Lewis acids—also led to equimolar mixtures of stereoisomers. In contrast, oxidation to pyridine-*N*-oxide **11** effectively differentiated prochiral faces of the pyridine and led to diastereoselective hydrogenation using Rh/Al_2O_3 (7:1 dr on gram scale). Stereoselectivity may reflect conformational restriction (see SI) or two-point binding of the Lewis basic *N*-oxide/ *N*-hydroxylamine and ether oxygen to the metal surface to direct hydrogen delivery to one face. The resistance of the N-O bond to hydrogenolysis was evidenced by persistence of *N*-hydroxypiperidine **14**, which could be cleanly reduced to **12** *in situ* by the addition of Zn. This single-atom structural change[35] to solve the problem of diastereoselective heteroarene hydrogenation complements prior approaches—chiral auxiliaries,[36] chiral catalysts,[37] covalent conformational locks[38]—and provides an alternative strategy for related systems. Fast, chemoselective reduction of the pyridine ring occurred until late in the reaction when small amounts of ketone reduction were observed, but the resulting alcohol byproduct was separable by chromatography on deactivated Al_2O_3.

Having solved the three main challenges of the synthesis—the unprecedented core, the strained ether, the *endo*-attached-rings—completion of the synthesis became straightforward. Ketone **12** was converted via Barton iodination to its corresponding vinyl iodide, which could be elaborated to the methyl ester using palladium-catalyzed carbonylation. Each step scaled to multigram quantities with few changes to the small-scale procedures. The brevity of the route allowed production of 2.5 grams (1 gram in 1 pass) of *rac*-**GB18** in an academic setting. The two enantiomers could be separated by preparative chiral SFC, crystallized to verify the absolute configuration of each antipode ((+)-*nat*-**GB18** and (–)-*ent*-**GB18**) and assayed to determine potential central nervous system targets.

GB18 had been singled out by Smith, Kline and French as a potential psychotropic principle of *Galbulimima* sp. due to its inhibition of mouse preening (5 mg/kg) without effect on the pain threshold.[6] Both *nat*-**GB18** and *ent*-**GB18** were therefore screened by the NIMH Psychoactive Drug Screening Program to identify high affinity targets among human receptors commonly involved in CNS modulation.[39] Whereas *nat*-**GB18** showed low or statistically-insignificant ($p > 0.05$) binding at 10 μM to 43 common drug targets including muscarinic receptors $M_{1–5}$, it strongly displaced [^{3}H]U-69593 (87%, $p \leq 0.001$) from *kappa*-opioid receptors (KOR) and [^{3}H]DAMGO (85%, $p \leq 0.001$) from *mu*-opioid receptors (MOR). Follow-up TANGO assays[40] identified *nat*-GB18 as a potent antagonist at both KOR (IC_{50} = 9 nM) and MOR (IC_{50} = 12 nM) (Figure 4b, red curve), comparable to the morphine derivative naltrexone (Figure 4b, blue curve). *Delta*- (DOR) and nociceptin opioid receptors (NOP) were not strongly ligated nor were Mas-related GPCRs. *ent*-GB18

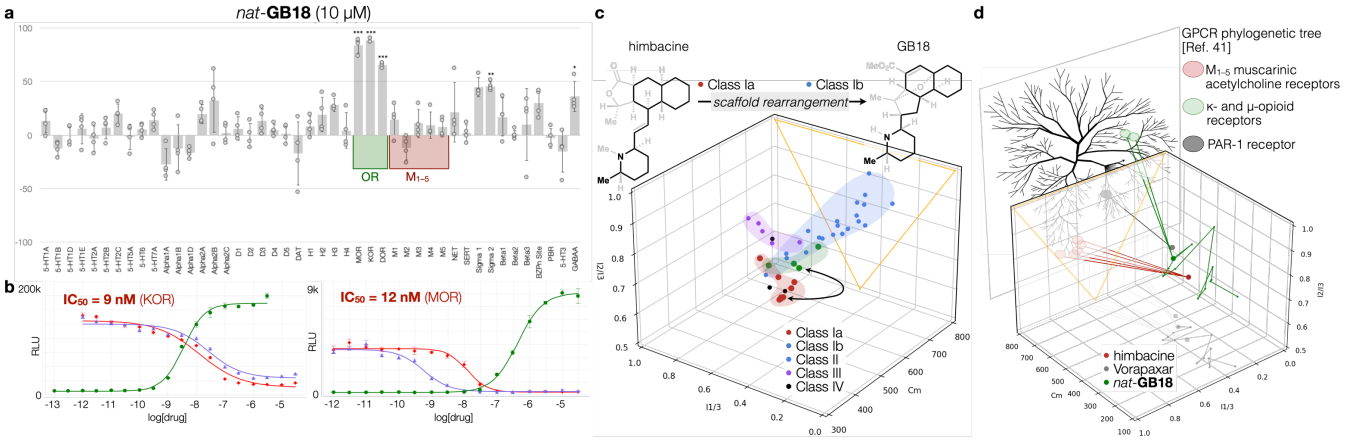

Figure 4. Identification of high potency target receptors of GB18. **a**. *nat*-**GB18** (*nat*-**1**) selectively ligates opioid receptors among 45 common receptors of neuroactive substances and potently antagonizes κ- and μ-opioid receptors.[39] Values indicate % inhibition of radioligand binding by 10 μM of (+)-*nat*-**1** ($n = 4$); *** $p \leq 0.001$, ** $p \leq 0.01$, * $p \leq 0.05$, two-tailed test (see SI for data tables); error bars indicate standard deviations. **b**. TANGO βarrestin signaling dose-response ($n = 3$).[40] KOR: salvinorin A (green), naltrexone (blue), *nat*-**GB18** (red); MOR: DAMGO (green), naltrexone (blue), *nat*-**GB18** (red). **c**. A chemical space (principal moment of inertia, PMI, and additive complexity, C_m) to distinguish the forty GB alkaloids that differ by piperidine-decalin topology, including himbacine and GB18. **d**. A walk through this chemical space to quickly access GB18 with the potential to perturb selectivity (KOR/MOR) among the GPCR phylogenetic tree, by analogy to himbacine ($M_{1–5}$) and Vorapaxar (PAR1). n = X number of concentration replicates; KOR = *kappa*-opioid receptor; MOR = *mu*-opioid receptor; DAMGO = [D-Ala^2, *N*-MePhe^4, Gly-ol^5]-enkephalin; GPCR = G protein-coupled receptor.

displaced [^{3}H]U-69593 from KOR with moderate affinity (56% at 10 μM, $p \leq 0.001$; K_i = 1.1 μM) and showed higher affinity to σ_1 and σ_2 receptors (see SI). The identification of MOR and KOR as high-affinity receptors for GB18 represent the first new target assignment for the GB alkaloids in over 35 years since the identification of himbacine as a muscarinic receptor antagonist.[7]

Overall homology among the GB alkaloids illustrates how the relatively small structural differences between himbacine and GB18, both Class I alkaloids, impart changes to binding affinity among rhodopsin-like GPCRs ($M_{1–5}$, subfamily A18 *vs*. opioid receptors, subfamily A4).[41] A correlation between structure and GPCR selectivity is also demonstrated by himbacine *vs*. Vorapaxar (enantiomeric series, antagonist of PAR1, subfamily A15), and therefore may serve as an organizing principle to classify GB alkaloids by function (Figure 4c), suggesting potential to similarly expand GB18 among the GPCRome. Functional organization of the GB alkaloids according to affinity and selectivity for diverse neuron receptors—not merely muscarinic receptors—complements existing characterization by structure and biosynthesis, and may begin to explain the diverse nervous system effects ascribed to the GB alkaloids over 50 years ago.[6]

The robust synthesis platform described here relies on fundamental discoveries in chemoselective scaffold assembly, stereoselective cross-coupling and stereoselective attached-ring hydrogenation. The route quickly enters GB chemical space (Figure 4d)[16] and allows the exploration of both enantiomeric series, diverse heterocyclic attached-ring analogs and core functional groups—all of which are expected to affect GPCR affinity and selectivity. Further knowledge of the targets of the GB alkaloids and their analogs will allow a more accurate parameterization of chemical space to correlate structure and function. For now, GB18 itself is available freely and to all interested parties.

ASSOCIATED CONTENT

Supporting Information

The Supporting Information is available free of charge on the ACS Publications website. Experimental procedures and spectra are available (pdf).

AUTHOR INFORMATION

Corresponding Author

*rshenvi@scripps.edu

ACKNOWLEDGMENT

K_i determinations, receptor binding profiles, agonist and antagonist functional data were generously provided by the National Institute of Mental Health's Psychoactive Drug Screening Program, Contract # HHSN-271-2018-00023-C (NIMH PDSP). The NIMH PDSP is Directed by Bryan L. Roth MD, PhD at the University of North Carolina at Chapel Hill and Project Officer Jamie Driscoll at NIMH, Bethesda MD, USA. We thank Jason Chen, Brittany Sanchez and Quynh Nguyen Wong for assistance with separations and analysis. Dr. Milan Gembicky, Dr. Erika Samolova, Dr. Jake Bailey and the entire UCSD Crystallography Facility are acknowledged for X-ray crystallographic analysis. Dr. Laura Pasternack and Dr. Dee-Hua Huang are acknowledged for assistance with NMR spectroscopy. We thank Dr. Steven Crossley, Max Palkowitz, Brendyn Smith and Dr. Guanghu Tong for proofreading. Support was provided by the National Institutes of Health (R35 GM122606; S10 OD025208), the National Science Foundation (CHE 1856747) and the Skaggs Graduate School (fellowship to S.W.). A provisional patent has been filed: U.S. Patent Application No. 63/301,677.

REFERENCES

1. Rinner, U. Galbulimima alkaloids. *Alkaloids. Chem. Biol*. **2017**, *78*, 109–166.
2. Thomas, B, "*Galbulimima belgraveana* (F. Muell) Sprague, *galbulimima agara*." *Eleusis: Journal of Psychoactive Plants and Compounds* **1999**, *2*, 82–88.
3. Thomas, B. Psychoactive Properties of Galbulimima Bark. *J. Psychoactive Drugs* **2005**, *37*, 109–111.
4. Thomas, B. "*Galbulimima* bark and ethnomedicine in Papua New Guinea" **2006**, *49*, 57–59.
5. Thomas, B. "Psychoactive plant use in Papua New Guinea" *Science in New Guinea*, **2000**, 25, 33–59.
6. D. J. Collins, C. C. J. Culvenor, J. A. Lamberton, J. W. Loder, J. R. Price, "Pharmacology of alkaloids" in Plants for Medicines (Commonwealth Scientific and Industrial Research Organization (CSIRO), Melbourne, 1990), pp. 71–106.
7. Gilani, H.; Coblin, L.B. "The cardio-selectivity of himbacine: A muscarine receptor antagonist" *Naunyn-Schmiedeberg's Archives of Pharmacology* **1986**, *332*, 16.
8. Neumann, K. 1998. "The Synthesis of the Galbulimima Alkaloids Himgravine and Himbacine: Potential Therapeutic Agents for Alzheimer's Disease" TMR-Grants. FMBICT960878. Category 30 (B30).
9. Chackalamannil, S.; Doller, D.; McQuade, R.; Ruperto, V. "Himbacine analogs as muscarinic receptor antagonists—effects of tether and heterocyclic variations" *Bioorg. Med. Chem. Lett*. **2004**, *14*, 3967.
10. Heardown, M. J. *Expert Opin. Therap. Patents* **2002**, *12*, 863.
11. Wolde Mussie, E.; Ruiz, G. "Method for reducing intraocular pressure in the mammalian eye by the administration of muscarine antagonists" U.S. Class. 514/219, Patent # 5716952 (02 10 98).
12. Binns, S.; Dunstan, P. J.; Guise, G. B.; Holder, G. M.; Hollis, A. F.; McCredie, R. S.; Pinhey, J. T.; Prager, R. H.; Rasmussen, M.; Ritchie, E.; Taylor, W. C. "The Chemical Constituents of Galbulimima species" *Aust. J. Chem*. **1965**, *18*, 569.
13. Ritchie, E.; Taylor, W. C. The Galbulimima Alkaloids. In The Alkaloids; 1967; Vol. IX, pp 529–543.
14. Böttcher, T. "An additive definition of molecular complexity" *J. Chem. Inf. Model*. **2016**, *56*, 462–470.
15. K. K. Larson, R. Sarpong, "Total synthesis of alkaloid (+/-)-G. B. 13 using a Rh(I)-catalyzed ketone hydroarylation and late-stage pyridine reduction" *J. Am. Chem. Soc*. **2009**, *131*, 13244– 13245.
16. Landwehr, E. M.; Baker, M. A.; Oguma, T.; Burdge, H. E.; Kawajiri, T.; Shenvi, R. A. "Concise syntheses of GB22, GB13 and himgaline by cross-coupling and complete reduction" *Science*, **2022**, *accepted,* abn8343.
17. Klix, R. C.; Bach, R. D. 1,2-Carbonyl Migrations in Organic Synthesis. An Approach to the Perhydroindanones. *J. Org. Chem*. **1987**, 52, 580–586.
18. Torii, S.; Okumoto, H.; Nakayasu, S.; Kotani, T. Hydrogenolysis of α,β-Epoxyketone and Ester to Aldol in Pd(0)/HCOOH/Et3N and H2/Pd/C Reduction Media. *Chem. Lett*. **1989**, 1975-1978.
19. Danheiser, R. L.; Carini, D. J.; Basak, A. (Trimethylsilyl)Cyclopentene Annulation: A Regiocontrolled Approach to the Synthesis of Five-Membered Rings. *J. Am. Chem. Soc*. **1981**, *103*, 1604–1606.
20. Ma, X.; Dang, H.; Rose, J. A.; Rablen, P.; Herzon, S. B. "Hydroheteroarylation of Unactivated Alkenes Using N-Methoxyheteroarenium Salts" *J. Am. Chem. Soc*. **2017**, *139*, 5998–6007.
21. Fu, G. C. "Transition-Metal Catalysis of Nucleophilic Substitution Reactions: A Radical Alternative to SN1 and SN2 Processes" *ACS Cent. Sci*. **2017**, *3*, 692–700.
22. Blackburn, J. M.; Roizen, J. L. "Catalytic Strategies to Convert 2-Halopyridines to 2-Alkylpyridines" *Asian J. Org. Chem*. **2019**, *8*, 920–930.
23. Nimmagadda, S.K.; Korapati, S.; Dasgupta, D.; Malik, N.A.; Vinodini, A.; Gangu, A.S.; Kalidindi, S.; Maity, P.; Bondigela, S.S.; Venu, A.; Gallagher, W.P. "Development and execution of an Ni (II)-catalyzed reductive cross-coupling of substituted 2-chloropyridine and ethyl 3-chloropropanoate." *Org. Process Res. Dev*. **2020**, *24*, 1141–1148.
24. Everson, D. A.; Weix, D. J. "Cross-Electrophile Coupling: Principles of Reactivity and Selectivity" *J. Org. Chem*. **2014**, *79*, 4793–4798.
25. Poremba, K. E.; Dibrell, S. E.; Reisman, S. E. "Nickel-Catalyzed Enantioselective Reductive Cross-Coupling Reactions" *ACS Catal*. **2020**, *15*, 8237.
26. Zhang, P.; Le, C.; Macmillan, D. W. C. "Silyl Radical Activation of Alkyl Halides in Metallaphotoredox Catalysis: A Unique Pathway for Cross-Electrophile Coupling" *J. Am. Chem. Soc*. **2016**, *138*, 8084–8087.
27. Hansen, E. C.; Li, C.; Yang, S.; Pedro, D.; Weix, D. J. "Coupling of Challenging Heteroaryl Halides with Alkyl Halides via Nickel-Catalyzed Cross-Electrophile Coupling." *J. Org. Chem*. **2017**, *82*, 7085–7092.
28. Anka-Lufford, L. L.; Huihui, K. M. M.; Gower, N. J.; Ackerman, L. K. G.; Weix, D. J. Nickel-Catalyzed Cross-Electrophile Coupling with Organic Reductants in Non-Amide Solvents. *Chem. - A Eur. J*. **2016**, *22*, 11564–11567.
29. Charboneau, D. J.; Huang, H.; Barth, E. L.; Germe, C. C.; Hazari, N.; Mercado, B. Q.; Uehling, M. R.; Zultanski, S. L. Tunable and Practical Homogeneous Organic Reductants for Cross-Electrophile Coupling. *J. Am. Chem. Soc*. **2021**, *143*, 21024–21036 .
30. S. A. Green, T. R. Huffman, R. O. McCourt, V. van der Puyl and R. A. Shenvi, *J. Am. Chem. Soc*. **2019**, *141*, 7709-7714.
31. S. L. Shevick, C. Obradors and R. A. Shenvi, *J. Am. Chem. Soc*. **2018**, *140*, 12056-12068.

32. Shevick, S. L.; Wilson, C. V.; Kotesova, S.; Kim, D.; Holland, P. L.; Shenvi, R. A. “Catalytic hydrogen atom transfer to alkenes: a roadmap for metal hydrides and radicals” *Chem. Sci.* **2020**, 12401–12422.
33. We excluded a hydroarylation mechanism by subjection of the alkene corresponding to **3** to coupling conditions (see SI); no products of cross-coupling were observed.
34. Hansen, E. C.; Pedro, D. J.; Wotal, A. C.; Gower, N. J.; Nelson, J. D.; Caron, S.; Weix, D. J. “New ligands for nickel catalysis from diverse pharmaceutical heterocycle libraries” *Nature Chem.* **2016**, *8*, 1126.
35. Boger, D. L. "The Difference a Single Atom Can Make: Synthesis and Design at the Chemistry–Biology Interface" *J. Org. Chem.* **2017**, *82*, 11961–11980.
36. Glorius, F.; Spielkamp, N.; Holle, S.; Goddard, R.; Lehmann, C. W. “Efficient Asymmetric Hydrogenation of Pyridines” *Angew. Chem. Int. Ed.* **2004**, *43*, 2850–2852.
37. Welin, E. R.; Ngamnithiporn, A.; Klatte, M.; Lapointe, G.; Pototschnig, G. M.; McDermott, M. S. J.; Conklin, D.; Gilmore, C. D.; Tadross, P. M.; Haley, C. K.; Negoro, K.; Glibstrup, E.; Grünanger, C. U.; Allan, K. M.; Virgil, S. C.; Slamon, D. J.; Stoltz, B. M. “Concise total syntheses of (-)-jorunnamycin A and (-)-jorumycin enabled by asymmetric catalysis” *Science* **2019**, *363*, 270–275.
38. Horii, Z.; Yamawaki, Y.; Hanaoka, M.; Tamura, Y.; Saito, S.; Yoshikawa, H. “Synthesis and Stereochemistry in B/C Ring Juncture of Lactam-carbinol A, a Degradation Product of Securinine” *Chem. Pharm. Bull.* **1965**, *13*, 22–26.
39. Besnard J.; Ruda G. F., Setola V.; Abecassis, K.; Rodriguiz, R. M.; Huang, X. P.; Norval, S.; Sassano, M. F.; Shin, A. I.; Webster, L. A.; Simeons, F. R.; Stojanovski, L.; Prat, A.; Seidah, N. G.; Constam, D.; Bickerton, G. R.; Read, K. D.; Wetsel, W. C.; Gilbert, I. H.; Roth, B. L.; Hopkins, A. L. "Automated design of ligands to polypharmacological profiles" *Nature, **2012**, 492,* 215–220.
40. Kroeze WK, Sassano MF, Huang XP, Lansu K, McCorvy JD, Giguère PM, Sciaky N, Roth BL. "PRESTO-Tango as an open-source resource for interrogation of the druggable human GPCRome" *Nat. Struct. Mol. Biol.* **2015**, *22*, 362–369.
41. Stevens, R. C.; Chezerov, V.; Katritch, V.; Abagyan, R.; Kuhn, P.; Rosen, H.; Wüthrich, K. "The GPCR Network: a large-scale collaboration to determine human GPCR structure and function" *Nat. Rev. Drug. Discov.* **2013**, *12*, 25–34.